

## THE COMPLETE SURVEY OF STAR-FORMING REGIONS: PHASE I DATA

NAOMI A. RIDGE,<sup>1</sup> JAMES DI FRANCESCO,<sup>2</sup> HELEN KIRK,<sup>2,3</sup> DI LI,<sup>1,4</sup> ALYSSA A. GOODMAN,<sup>1</sup> JOÃO F. ALVES,<sup>5</sup>  
HÉCTOR G. ARCE,<sup>6</sup> MICHELLE A. BORKIN,<sup>7</sup> PAOLA CASELLI,<sup>8</sup> JONATHAN B. FOSTER,<sup>1</sup> MARK H. HEYER,<sup>9</sup>  
DOUG JOHNSTONE,<sup>2,3</sup> DAVID A. KOSSLYN,<sup>1</sup> MARCO LOMBARDI,<sup>4</sup> JAIME E. PINEDA,<sup>1</sup>  
SCOTT L. SCHNEE,<sup>1</sup> AND MARIO TAFALLA<sup>10</sup>

Received 2005 November 8; accepted 2006 February 22

### ABSTRACT

We present an overview of data available for the Ophiuchus and Perseus molecular clouds from Phase I of the COMPLETE Survey of Star-Forming Regions. This survey provides a range of data complementary to the *Spitzer* Legacy Program “From Molecular Cores to Planet Forming Disks.” Phase I includes the following: extinction maps derived from the Two Micron All Sky Survey (2MASS) near-infrared data using the NICER algorithm; extinction and temperature maps derived from *IRAS* 60 and 100  $\mu\text{m}$  emission; H I maps of atomic gas;  $^{12}\text{CO}$  and  $^{13}\text{CO}$  maps of molecular gas; and submillimeter continuum images of emission from dust in dense cores. Not unexpectedly, the morphology of the regions appears quite different depending on the column density tracer that is used, with *IRAS* tracing mainly warmer dust and CO being biased by chemical, excitation, and optical depth effects. Histograms of column density distribution are presented, showing that extinction as derived from 2MASS NICER gives the closest match to a lognormal distribution, as is predicted by numerical simulations. All the data presented in this paper, and links to more detailed publications on their implications, are publicly available at the COMPLETE Web site.

*Key words:* ISM: clouds — stars: formation — surveys

### 1. INTRODUCTION

The prevailing theoretical picture of star formation envisions stars forming within dense cores, which are embedded in turn within larger, slightly lower density structures. Each forming star is surrounded by a disk, and, when it is very young, the star-disk system produces a collimated bipolar flow in a direction perpendicular to the disk. In its broad outlines, this paradigm is very likely to be correct. In detail, however, many questions remain concerning the timing of this series of events. For example, how long does a star stay with its natal core? How long does it remain associated with the lower density structure (e.g., a filament in a dark cloud) in which it originally formed? What kind of environment does a star-disk system need to keep accreting or to produce an outflow, and when might that reservoir no longer be available to the system? Does a bipolar outflow have any effect on star formation nearby? What causes fragmentation into binaries or higher order systems? How much influence do spherical winds (e.g.,

supernovae, B star winds) from previous generations of stars have on the timing of star formation? How often is a star in the process of forming likely to encounter an external gravitational potential (e.g., from another forming star) strong enough to alter its formation process? The complicating issue underlying all of these questions is that it is hard to define and understand the properties of the reservoir from which a star forms if the reservoir itself is highly dynamic.

The COMPLETE (Coordinated Molecular Probe Line Extinction and Thermal Emission)<sup>11</sup> Survey of Star-Forming Regions is intended to provide an unprecedented comprehensive database with which one might have real hope of answering many statistically addressable questions about star formation. Its primary goal is to provide detailed measurements of the velocity fields (from molecular line observations), the density profiles (from extinction measurements), the temperature and dust property profiles (from thermal emission mapping), the larger cloud environment (from atomic hydrogen), and the embedded source distributions (from infrared imaging) of several nearby molecular clouds.

COMPLETE is not the first such study of this kind: Lada (1992) mapped the actively star-forming cloud L1630 (a.k.a. Orion B) both in molecular line emission (CS, with 2' resolution) and with near-infrared cameras (reaching  $m_K < 13$  mag). That work provided the first evidence that massive stars form in clusters, and it also showed that the mass spectrum of the gaseous material (self-gravitating or not) is shallower than that for stars. COMPLETE, which was not feasible a decade ago, is intended to allow for low-mass (fainter) star-forming regions what Lada's work allowed for (brighter) massive star-forming regions, and more. For reference, the total areal coverage of COMPLETE is  $\sim 20$  deg<sup>2</sup>, which is an order of magnitude larger than the area Lada studied in Orion.

<sup>1</sup> Harvard-Smithsonian Center for Astrophysics, 60 Garden Street, Cambridge, MA 02138.

<sup>2</sup> National Research Council of Canada, Herzberg Institute of Astrophysics, 5071 West Saanich Road, Victoria, BC V9E 2E7, Canada.

<sup>3</sup> Department of Physics and Astronomy, University of Victoria, P.O. Box 3055, Station CSC, Victoria, BC V8P 1A1, Canada.

<sup>4</sup> Jet Propulsion Laboratory, California Institute of Technology, 4800 Oak Grove Drive, Pasadena, CA 91109.

<sup>5</sup> European Southern Observatory, Karl-Schwarzschild-Strasse 2, D-85748 Garching bei München, Germany.

<sup>6</sup> Department of Astrophysics, American Museum of Natural History, New York, NY 10024.

<sup>7</sup> Department of Astronomy, Harvard University, 60 Garden Street, Cambridge, MA 02138.

<sup>8</sup> INAF—Osservatorio Astrofisico di Arcetri, Largo Enrico Fermi 5, 50125 Florence, Italy.

<sup>9</sup> Department of Astronomy, University of Massachusetts, Lederle Graduate Research Center, Amherst, MA 01003.

<sup>10</sup> Observatorio Astronómico Nacional, Alfonso XII 3, E-28014 Madrid, Spain.

<sup>11</sup> The COMPLETE Web site is at <http://www.cfa.harvard.edu/COMPLETE>.

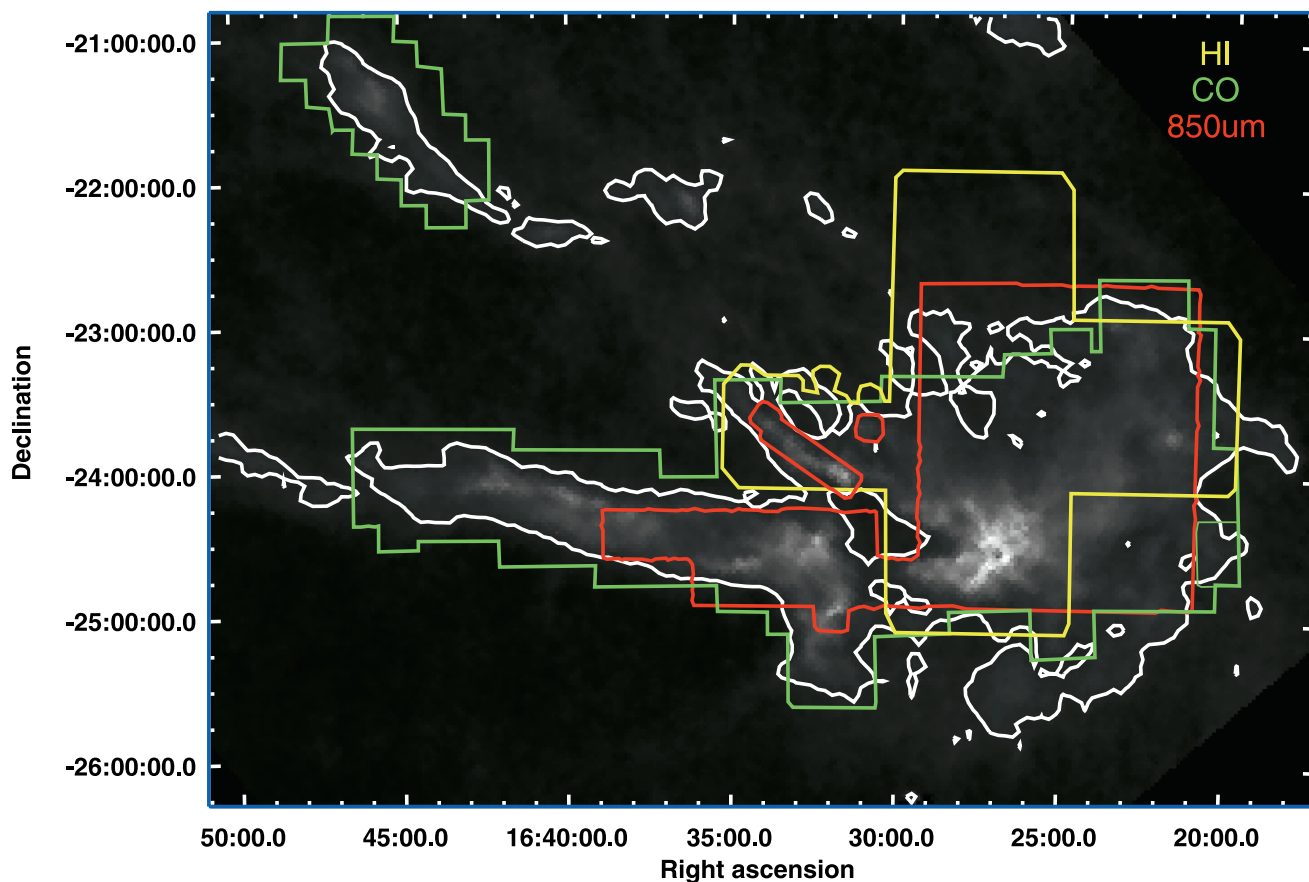


FIG. 1.—2MASS NICER extinction map of Ophiuchus overlaid with outlines showing the areas covered by  $^{12}\text{CO}$  and  $^{13}\text{CO}$  observations (green),  $850\ \mu\text{m}$  continuum observations (red), and H I observations (yellow), which are all available to download from the COMPLETE Web site. Note that the small “hole” at the center of the L1689 cluster is an artifact due to the high extinction at that position. The white contour indicates an  $A_V$  of 3 mag.

COMPLETE makes it possible for researchers to combine diverse observational techniques and to measure the physical properties of the three star-forming clouds Perseus, Ophiuchus, and Serpens. These three were chosen because they are nearby extended cloud targets, were also included in the *Spitzer Space Telescope* “From Molecular Cores to Planet Forming Disks” (c2d) Legacy Program (Evans et al. 2003), and are visible from Northern Hemisphere observatories. Selecting such targets from c2d ensured that full censuses of their embedded stellar populations and their properties would be available around the same time that COMPLETE was finished.

COMPLETE was designed to be executed in two phases. Phase I focuses on observing the “larger context” of the star formation process (on 0.1–10 pc scales). All of the Perseus and Ophiuchus cloud area to be observed with *Spitzer* under c2d, and slightly more, has already been covered by COMPLETE in an unbiased way for Phase I. Observations of the third cloud, Serpens, are less advanced and hence are not included here.<sup>12</sup> Phase II, which is already well underway, will be a statistical study of the small-scale picture of star formation, aimed at assessing the meaning of the variety of physical conditions observed in star-forming cores (on the  $<0.1$  pc scale). In Phase II, targeted source lists based on the Phase I data are being used, as it is (still) not feasible to cover every dense star-forming peak at high resolution. These

data are being released on the COMPLETE Web site as they are validated.

In this paper we present an overview of the Phase I data of COMPLETE for the Ophiuchus and Perseus clouds, which include the following: extinction maps derived from near-infrared data; extinction and temperature maps derived from *IRAS* 60 and  $100\ \mu\text{m}$  emission; emission maps of atomic line data (H I); emission maps of molecular line data ( $^{12}\text{CO}$  and  $^{13}\text{CO}$ ); and emission maps of submillimeter continuum data. Section 2 gives a description of the data acquisition and reduction techniques for each data set. Detailed analyses and interpretation of these data appear elsewhere (e.g., Johnstone et al. 2004; Walawender et al. 2005; Schnee et al. 2005, 2006; Ridge et al. 2006; A. A. Goodman et al. 2006, in preparation; N. A. Ridge et al. 2006, in preparation; Kirk et al. 2006). All Phase I COMPLETE data are publicly available and can be retrieved from the COMPLETE Web site.

## 2. DATA AND OBSERVATIONAL FINDINGS

Figures 1 and 2 show the 2MASS near-infrared color excess revisited (NICER) extinction maps for Ophiuchus and Perseus (see § 2.1) overlaid with the boundaries of the associated regions surveyed in molecular lines, thermal dust emission, and H I emission, as described in the remainder of this section. COMPLETE coverage was chosen to coincide with the coverage of c2d Infrared Array Camera observations and to include most areas with  $A_V > 3$  mag (Figs. 1 and 2, white contours) and all with

<sup>12</sup> Serpens data are available at the COMPLETE Web site, however.

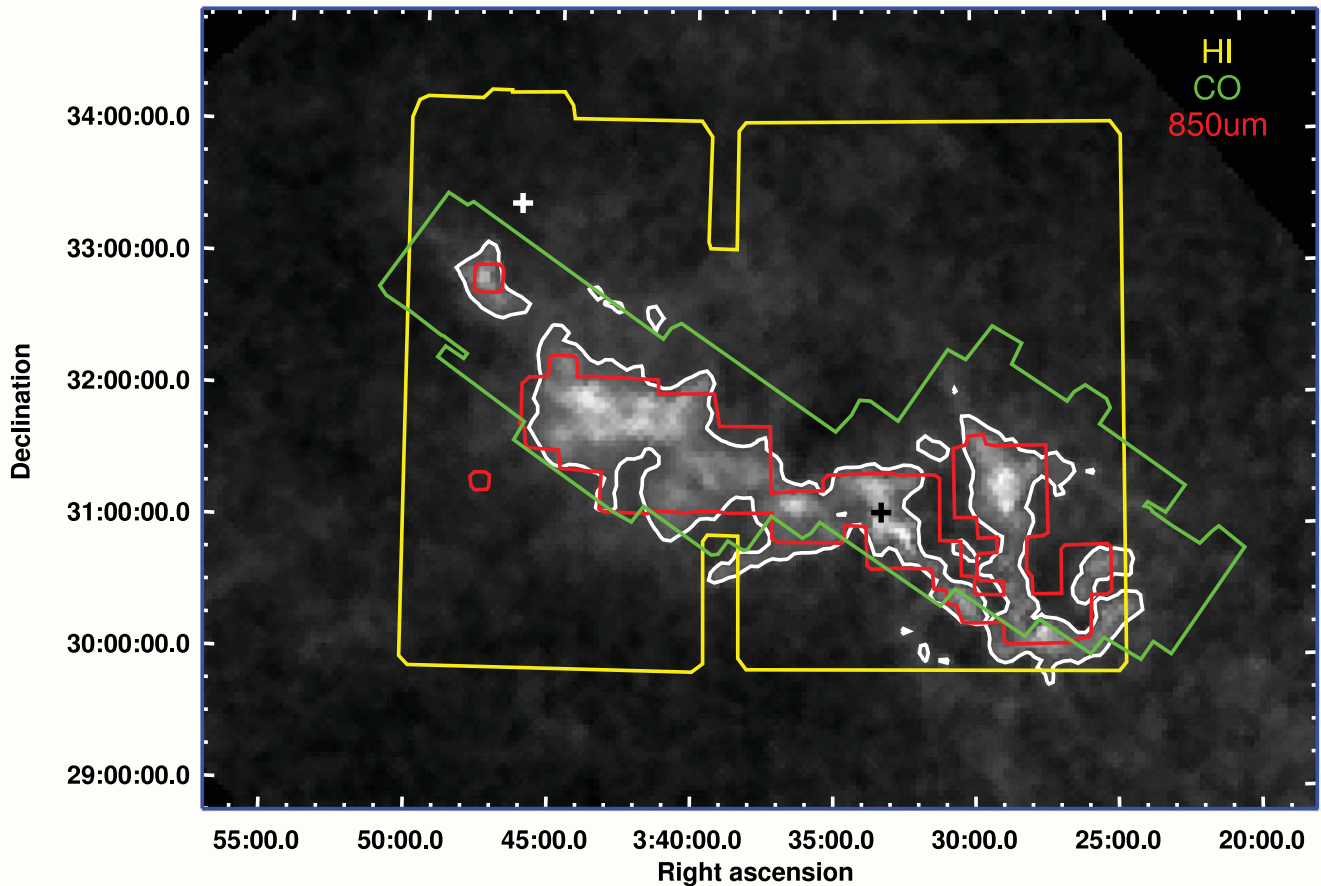


FIG. 2.—2MASS NICER extinction map of Perseus overlaid with outlines showing the areas covered by  $^{12}\text{CO}$  and  $^{13}\text{CO}$  observations (green),  $850\ \mu\text{m}$  continuum observations (red), and H I observations (yellow), which are all available to download from the COMPLETE Web site. The white contour indicates an  $A_V$  of 3 mag. The black and white crosses indicate the positions of the spectra shown in Figs. 10 and 11, respectively.

$A_V > 5$  mag. Table 1 summarizes the basic physical properties of the two star-forming regions.

### 2.1. Extinction Maps from 2MASS

Near-infrared extinction maps for Ophiuchus and Perseus were produced from the final data release of the point source catalog from the Two Micron All Sky Survey.<sup>13,14</sup> We used the NICER algorithm (Lombardi & Alves 2001, 2006), which

combines observations from all three near-infrared bands to produce maps with lower noise than is possible from using just two bands. The NICER algorithm takes advantage of the small variation in the intrinsic colors of stars in the near-infrared to obtain an accurate estimate of the column density toward each star. In particular, the colors of all 2MASS stars in the field are compared to the colors of (supposedly) unreddened stars in a control field; then, for each star, an optimal combination of near-infrared colors is determined by taking into account the different response of the various colors to the reddening, the photometric errors on the star magnitudes, and the dispersion of intrinsic colors (as determined from the control field; see Lombardi & Alves [2001] for further details). Note that for the NICER analysis we used a normal reddening law (Rieke & Lebofsky 1985); interestingly,

<sup>13</sup> The 2MASS project is a collaboration between the University of Massachusetts and the Infrared Processing and Analysis Center (JPL, Caltech). Funding is provided primarily by NASA and the NSF.

<sup>14</sup> See <http://www.ipac.caltech.edu/2mass/releases/allsky/doc/explsup.html>.

TABLE 1  
OPHIUCHUS AND PERSEUS PHYSICAL PROPERTIES

Cloud	Distance <sup>a</sup> (pc)	Total Gas Mass <sup>b</sup> ( $M_\odot$ )	Size <sup>c</sup> ( $\text{pc}^2$ )	References
Ophiuchus .....	$125 \pm 25$	$7.4 \times 10^3$	46	de Geus et al. (1989)
Perseus .....	$250 \pm 50$	$1.0 \times 10^4$	70	Enoch et al. (2006)

<sup>a</sup> We quote the distances adopted by the c2d team for each of the clouds (N. Evans 2005, personal communication).

<sup>b</sup> Total mass enclosed within the  $A_V = 3$  mag contour, as determined from the 2MASS NICER extinction map.

<sup>c</sup> Total area enclosed within the  $A_V = 3$  mag contour, as determined from the 2MASS NICER extinction map.

TABLE 2  
2MASS NICER DATA

Parameter	Ophiuchus	Perseus
Pixel size (arcmin).....	1.5	2.5
Effective resolution (arcmin).....	3	5
Areal coverage (deg).....	9 × 8	9 × 12
1 $\sigma$ noise ( $A_V$ ).....	0.16	0.18

this reddening law compares well with the newly determined 2MASS reddening law (Indebetouw et al. 2005; see also Lombardi et al. 2006).

At the end of this preliminary step, we have a catalog of extinction measurements (and relative errors) for each star. These pencil-beam estimates then need to be interpolated in order to produce a smooth map and to reduce their variance. In particular, we smoothed the data using the moving average technique using a Gaussian kernel. This simple smoothing algorithm has easily quantified error properties (e.g., it is possible to easily determine the error map)<sup>15</sup> and works well for nearby objects such as those in COMPLETE, where background stars constitute the vast majority of all stars and do not force us to either clip out high- $\sigma$  (foreground) stars or employ the more robust weighted median, both of which would lead to more complicated error properties. Smoothed in this way, the map is really the convolution of the true extinction with the weighting function, and so it is not sensitive to spatial scales smaller than the weighting function (see Lombardi & Schneider 2001).

In Perseus, we produced an extinction map that is approximately  $9^\circ$  by  $12^\circ$ , with an effective resolution of  $5'$ . The average  $1\sigma$  noise in this image is 0.18 mag of  $A_V$ . Some remnant stripes are visible in the north-south direction of the 2MASS strips, reflecting errors in 2MASS calibration between strips. In Ophiuchus, our map is  $9^\circ$  by  $8^\circ$ , with an effective resolution of  $3'$  and an average  $1\sigma$  noise of 0.16 mag of  $A_V$ . Again, 2MASS stripes are visible. The properties of the maps are summarized in Table 2. A small hole is present in the center of L1688 in the Ophiuchus map, where 2MASS provides no data due to extremely high extinction (i.e.,  $A_V > 30$  mag).<sup>16</sup>

Several globular clusters, listed in Table 3, also show up in regions of relatively little extinction. Stars in these clusters are typically rather blue and thus produce slightly lower extinction values. The error map is useful for identifying these globular clusters, as well as star-forming clusters associated with either cloud, both of which bias the extinction determination but show up in the error map as regions of very low error, since the stellar density is high (Lombardi & Alves 2006). The final extinction maps, with the locations of the well-known dense cores and star-forming clusters in the two regions indicated, are shown in Figures 3 and 4.

The map of Ophiuchus reveals its multifilamentary structure well; starting from the very opaque L1688<sup>17</sup> to the west, two filaments can be seen, a northeastern filament (including L1740) and a less tenuous eastern filament containing the L1729, L1712, and L1689 Lynds clouds. The northeast filament appears the lon-

<sup>15</sup> See [http://cfa-www.harvard.edu/COMPLETE/data.html\\_pages/2MASS.html](http://cfa-www.harvard.edu/COMPLETE/data.html_pages/2MASS.html).

<sup>16</sup> Deeper near-infrared observations being obtained as part of Phase II will fill such holes.

<sup>17</sup> The bright extinction peak we have labeled “L1688” also includes L1686, L1692, L1690, and L1681.

TABLE 3  
GLOBULAR CLUSTERS THAT AFFECT THE OPHIUCHUS EXTINCTION MAP

Name	R.A.	Decl.
NGC 6235.....	16 53 25.36	−22 10 38.8
NGC 6144.....	16 27 14.14	−26 01 29.0
M80.....	16 17 02.51	−22 58 30.4
M4.....	16 23 35.41	−26 31 31.9

NOTE.—Units of right ascension are hours, minutes, and seconds, and units of declination are degrees, arcminutes, and arcseconds.

gest and has extinction maxima at each end associated with L1765 and L1709. L1688, where the filaments intersect, has the highest extinction in the Ophiuchus cloud. There is also an extension of L1688 to the northwest, containing L1687 and L1680.

The 2MASS NICER extinction map of Perseus (Fig. 4) shows the familiar chain of dark clouds from northeast to southwest. All of the known dark clouds and star-forming regions are seen, with the highest extinction regions corresponding to the two well-studied star-forming clusters IC 348 and NGC 1333.

Histograms showing the distribution of extinctions are shown in Fig. 5. Both the Ophiuchus and Perseus histograms show an approximately lognormal distribution of material (*curve*), as is predicted by numerical simulations (e.g., Ostriker et al. 2001). The physical implications of the measured column-density distributions will be discussed further in A. A. Goodman et al. (2006, in preparation), but note that due to the differing resolutions, the histograms presented are not directly comparable to those presented for the *IRAS* and CO data in subsequent sections.

## 2.2. Extinction and Temperature Maps from *IRAS*

IRIS<sup>18</sup> images (Miville-Deschênes & Lagache 2005) of 60 and 100  $\mu\text{m}$  flux density were obtained for the two regions. IRIS data offer excellent correction for the effects of zodiacal dust and striping in the unprocessed *IRAS* images and also provide improved gain and offset calibration over earlier releases (e.g., *IRAS* Sky Survey Atlas), which did not have an appropriate zero-point calibration. This can have serious consequences on the derived dust temperature and column density (Arce & Goodman 1999a, 1999b).

We used the method described in Schnee et al. (2005) (which is an adaptation of the method used by Wood et al. [1994] and Arce & Goodman [1999b]) to calculate the dust color temperature and column density from the IRIS 60 and 100  $\mu\text{m}$  flux densities. The temperature is determined by the ratio of the 60 and 100  $\mu\text{m}$  flux densities, assuming that the dust in a single beam is isothermal (the validity and implications of this assumption are discussed in detail in Schnee et al. 2005, 2006). The column density of dust can then be derived from measured flux and the derived color temperature of the dust. The calculation of temperature and column density depends on the values of three parameters: two constants that determine the emissivity spectral index and the conversion from 100  $\mu\text{m}$  optical depth to visual extinction. These parameters are solved for explicitly using the independent estimate of visual extinction we have from our 2MASS NICER extinction maps (described in § 2.1).

The 2MASS NICER extinction maps are used as a “model” of the extinction and the three free parameters adjusted until the IRIS-implied column density best matches that of the model. The

<sup>18</sup> Improved Recalibration of the *IRAS* Survey.

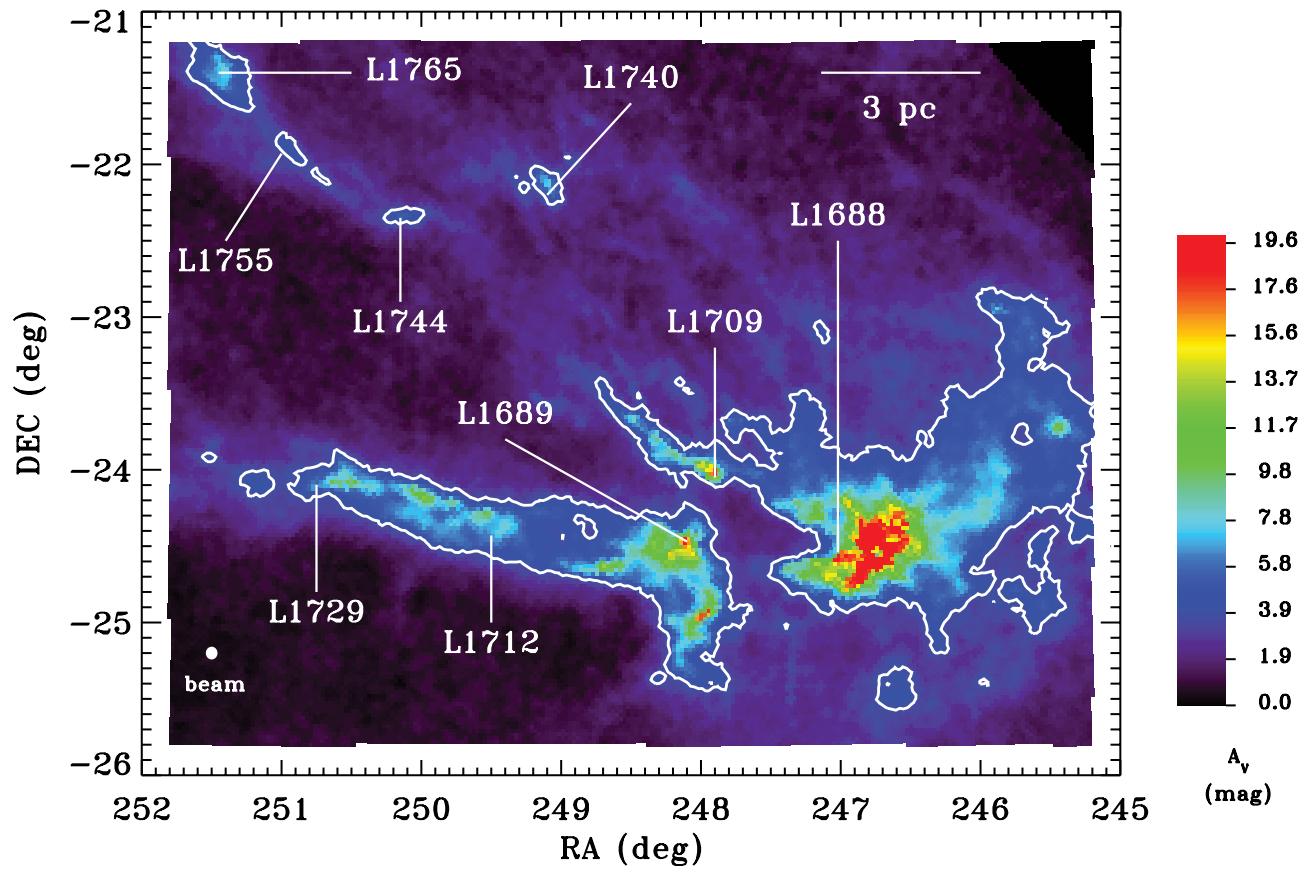


FIG. 3.—Map of extinction in Ophiuchus derived using 2MASS NICER. The contour indicates an  $A_V$  of 3 mag and is repeated in subsequent figures for orientation. Note that the small “hole” at the center of the L1688 cluster is an artifact due to the high extinction at that position.

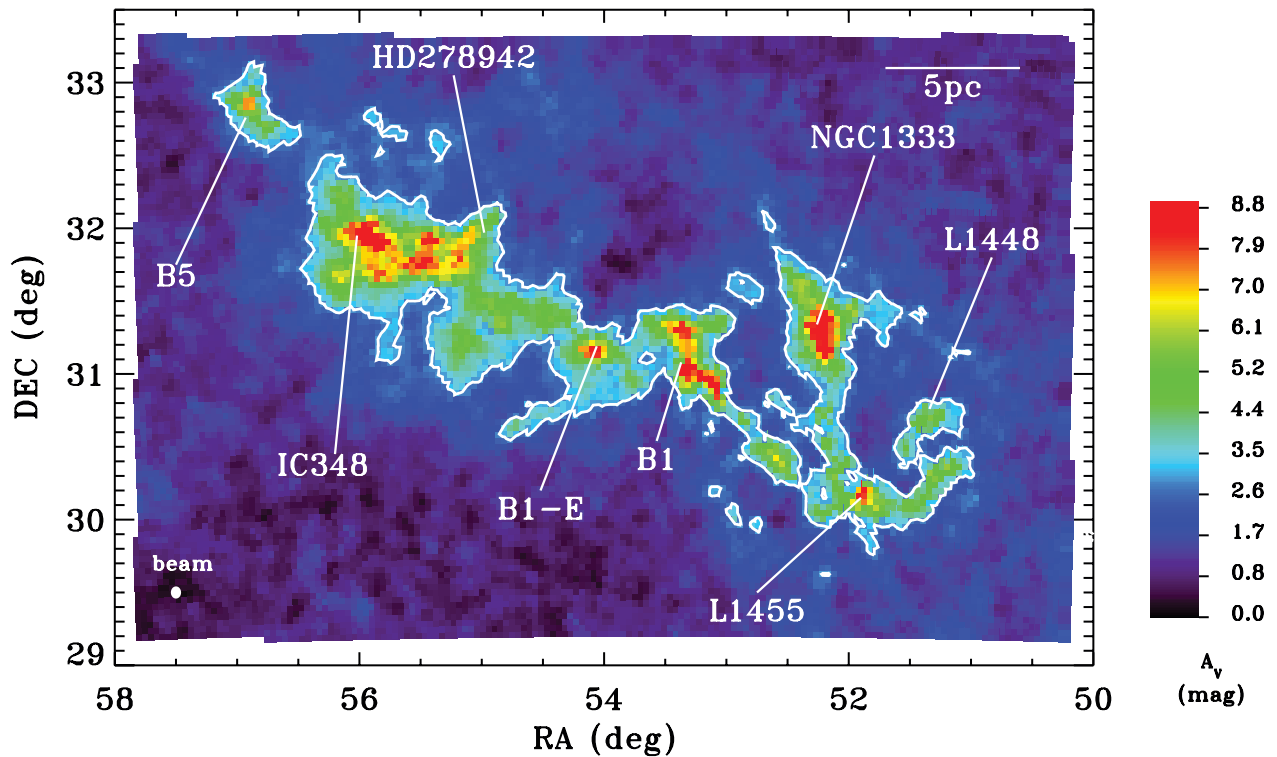


FIG. 4.—Map of extinction in Perseus derived using 2MASS NICER. The contour indicates an  $A_V$  of 3 mag and is repeated in subsequent figures for orientation. The well-known dark clouds and star-forming clusters in the region are labeled.

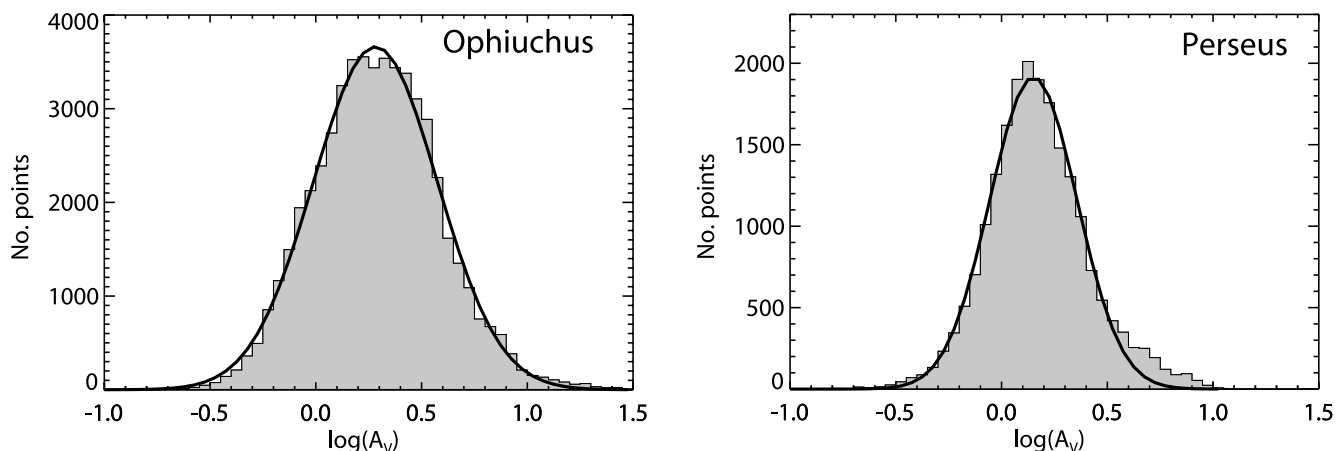


FIG. 5.—Histograms of extinction as derived from 2MASS in Ophiuchus (*left*) and Perseus (*right*) for the areas shown in Figs. 3 and 4 (*histograms*), with a lognormal fit to the data overlotted (*curve*).

parameter values determined by this method are those that create a far-IR-based extinction map that best matches the 2MASS NICER extinction map on a statistical point-by-point basis and is not a spatial match to features in the 2MASS NICER extinction map.

Each cloud is considered separately, so the derived values of the three parameters are different for each cloud. We assume that the values of the three parameters are constant within each image, although this does not have to be the case. For instance, it is likely that areas of especially high or low column density do not share the same far-IR column density-to-visual extinction conversion factor.

The *IRAS*-based extinction and temperature maps for Perseus and Ophiuchus are shown in Figures 6 and 7, and their properties are given in Table 4. The *IRAS*-based extinction map of Ophiuchus shows a general similarity to the 2MASS-based extinction map. Notable differences, however, include an extension of moderate extinction to the northwest of L1688 and a regular series of high-extinction peaks running west of L1689. Although there is some enhanced extinction northwest of L1688 in the 2MASS NICER map, this difference is likely an example of how the *IRAS*-based extinction maps can be biased toward warmer dust and possibly suggests warmer dust in that region due to external heating by the star  $\rho$  Oph itself (Schnee et al. 2005). A notable feature in the temperature map is a heated ring, visible just to the north of L1688 and centered on the B star  $\rho$  Oph.

Unlike in Ophiuchus, the *IRAS*-based extinction map of Perseus (Fig. 7, *left*) shows a vastly different morphology from the 2MASS NICER extinction map (on more careful inspection, and by comparison with the dust color-temperature map [Fig. 7, *right*], the known dark cores in Perseus are visible, however). This is because the column density as measured by *IRAS* is dominated by a  $0.75^\circ$  warm shell, probably caused by emission from transiently heated small dust grains at the edge of an H II region created by the B0 star HD 278942 (Ridge et al. 2006; Andersson et al. 2000).

Histograms showing the distribution of extinctions and temperatures in the two regions are shown in Figures 8 and 9. Detailed discussion of the histograms and a comparison of the histograms produced from *IRAS* and 2MASS NICER appear in Schnee et al. (2005) and A. A. Goodman et al. (2006, in preparation), respectively, but they are included here for completeness. Note that due to their differing resolution the histograms presented here are not

directly comparable with those presented for the 2MASS NICER extinction and CO data in §§ 2.1 and 2.4.

### 2.3. Atomic Hydrogen Maps from GBT

Maps of 21 cm H I emission over the Ophiuchus and Perseus clouds, covering 5 and 20 deg<sup>2</sup>, respectively, were obtained with the 100 m NRAO Green Bank Telescope (GBT)<sup>19</sup> in West Virginia over two observing runs in 2004 March and 2005 April. Both maps cover the densest cores in the regions, as well as regions of substantially lower density, where H I could be stronger in emission due to the prevalence of atomic hydrogen rather than molecular hydrogen. On-the-fly (OTF) mapping and frequency switching with a 1 MHz throw were used together with a data dumping rate of twice the Nyquist sampling rate, i.e., four dumps as the telescope moves over a whole beam. The 12.5 MHz total bandwidth mode of the GBT spectrometer was used with two spectral windows, one at 1420.4 MHz for H I, the other centered at 1666.4 MHz for the two OH  $\lambda$ -doubling lines at 1667.4 and 1666.4 MHz.<sup>20</sup> Each spectral window has two linear polarizations, for a total of four intermediate frequency (IF) inputs. With 16,384 lags, a 0.76 kHz channel width was achieved.

During reduction, frequency-switched data at both frequencies (+/- frequency throw) were treated independently because of instrument baseline stability. The data were reduced using IDL routines written by G. Langston that are consistent in terms of calibration when checked with AIPS++ packages provided by NRAO. Conversion to antenna temperature was achieved through scaling by a noise tube input, and conversion to absolute flux levels was achieved through comparisons with observations of Mars. Calibrated data were regridded to  $4'$  spacing in AIPS. The final data have an angular resolution of  $\sim 9'$  FWHM, a spectral resolution of 0.32 km s<sup>-1</sup>, and a typical  $1\sigma$  rms noise of 0.15 K per channel. The properties of the H I maps are summarized in Table 5. Three-dimensional fits files can be viewed online at the COMPLETE Web site: the value of these data is in the spectral information, and hence we do not show an integrated intensity map here. The angular resolution is comparable to the size of the dense structures in the two regions surveyed.

<sup>19</sup> NRAO (and the GBT) are operated by Associated Universities, Inc., under cooperative agreement with the NSF.

<sup>20</sup> The OH data will be presented in a future paper and are not discussed further here.

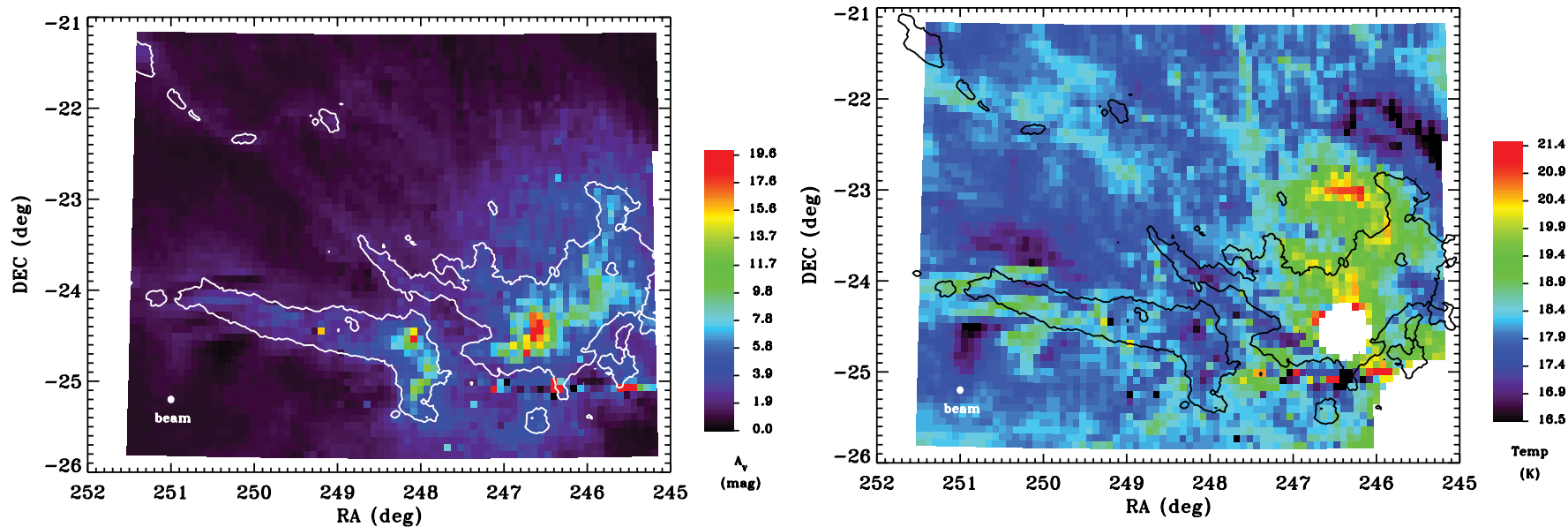


FIG. 6.—Column density (*left*) and temperature (*right*) in Ophiuchus derived from *IRAS*. The contour indicates an  $A_V$  value of 3 mag, as in Fig. 3.

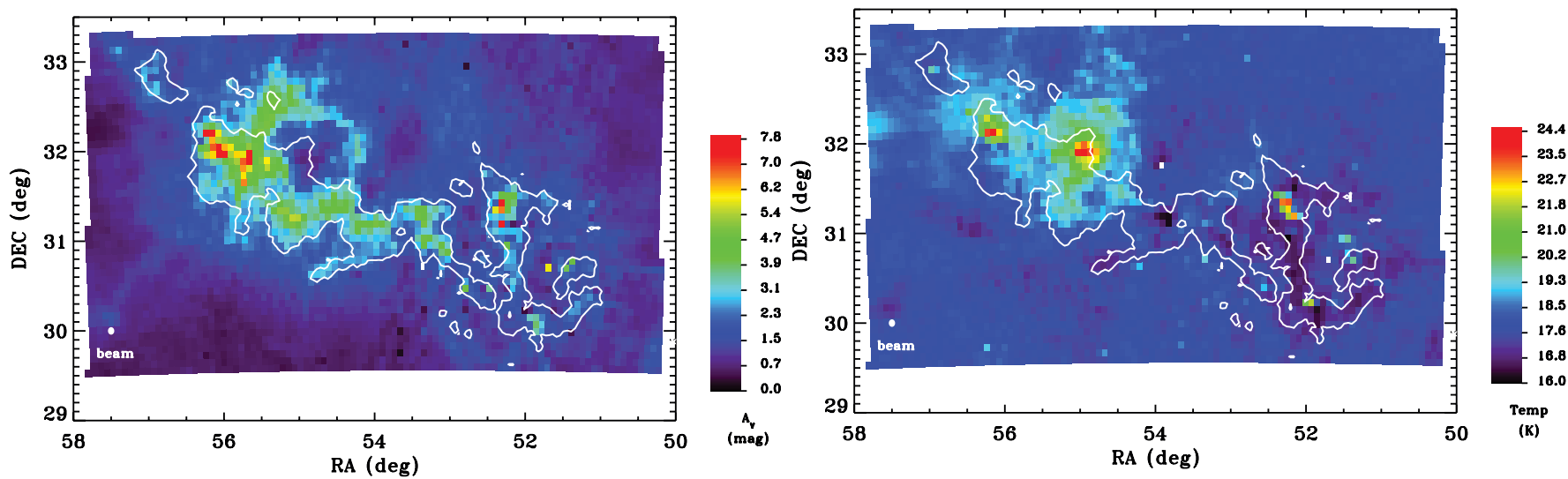


FIG. 7.—Column density (*left*) and temperature (*right*) in Perseus derived from *IRAS*. The contour indicates an  $A_V$  value of 3 mag, as in Fig. 4.

TABLE 4  
IRAS DATA

Parameter	Ophiuchus	Perseus
Pixel size (arcmin).....	5	5
Effective resolution (arcmin).....	5	5
Areal coverage (deg).....	6.3 × 6.4	7 × 4.5

The line profiles of H I in Ophiuchus reveal a strong and extensive H I narrow self-absorption (HINSA; Li & Goldsmith 2003) component, which is well correlated with molecular emission. This is consistent with previous pointed observations of the same region at a much lower resolution (Goodman & Heiles 1994). Channel maps of H I emission between 8 and 11 km s<sup>-1</sup> suggest a possible association of H I gas in this velocity range with the heated ring seen in the warm *IRAS* temperature map.

The main component of H I emission toward the line of sight of Perseus is centered around 4–8 km s<sup>-1</sup>, with the velocity of peak emission becoming redder toward the west of the region, as is seen in the molecular gas. The H I peaks, however, tend to be on the bluer side of the molecular gas by 1–2 km s<sup>-1</sup>. For example, around dense core B1, the H I emission shows approximately a single Gaussian profile with peak velocity at 4.8 km s<sup>-1</sup>, while <sup>13</sup>CO peaks at ~6.7 km s<sup>-1</sup> (Fig. 10).

The line-width of H I emission in Perseus is around 7–10 km s<sup>-1</sup> FWHM. Unlike other nearby regions, such as Taurus and Ophiuchus, the HINSA component is only seen toward a small portion of the dense clouds. This may be explained by viewing geometry and the different distances of the Perseus components. A minor, but very interesting, component in our Perseus map is the presence of high-velocity line wings in H I emission, extending from the main component all the way down to -50 km s<sup>-1</sup>, where it peaks up again to possibly reflect H I emission from another Galactic arm (Fig. 11). Although its origin is unclear at the moment, it is worth noting that it is probably too wide to be explained by a single low-level H I emission component somewhere else in the galaxy.

#### 2.4. Molecular Line Maps from FCRAO

Observations in the <sup>12</sup>CO 1–0 (115.271 GHz) and <sup>13</sup>CO 1–0 (110.201 GHz) transitions were carried out throughout the 2002–

2005 observing seasons at the 14 m Five College Radio Astronomy Observatory (FCRAO)<sup>21</sup> telescope in New Salem, Massachusetts. The SEQUOIA 32-element focal-plane array and an OTF mapping technique were used to make 10' × 10' submaps. The dual-IF narrowband digital correlator enabled <sup>12</sup>CO and <sup>13</sup>CO to be observed simultaneously. The correlator was used in a mode that provided a total bandwidth of 25 MHz with 1024 channels in each IF, yielding an effective velocity resolution of 0.07 km s<sup>-1</sup>. Data were taken during a wide range of weather qualities, and system temperatures were generally between 500 and 1000 K at 115 GHz and 200 and 600 K at 110 GHz (single sideband). Due to its low elevation, system temperatures for Ophiuchus were consistently higher than for Perseus. Submaps with higher system temperatures were repeated to achieve uniform sensitivity where possible.

The submaps were obtained by scanning in the right ascension direction,<sup>22</sup> and an off-source reference scan was obtained after every two or four rows, depending on weather and elevation. Off-positions were checked to be free of emission by making separate 10' OTF maps, with an off-position an additional 30' offset. Calibration was found via the chopper-wheel technique (Kutner & Ulich 1981), yielding spectra with units of T<sub>A</sub><sup>\*</sup>. Pointing was checked regularly and found to vary by less than 5" rms.

Due to Dewar rotation, the OTF data are not evenly sampled, and so a convolution and regridding algorithm has to be applied to the data to obtain spectra on a regularly sampled grid. This process was carried out on the individual 10' × 10' submaps using software provided by the observatory (Heyer et al. 2001). After subtraction of a linear baseline, each spectrum was convolved with nearby spectra onto a regular 23" grid weighted by rms<sup>-2</sup>, yielding a Nyquist-sampled map. The submaps were then combined into the final map using an IDL routine and corrected for the main beam efficiency (0.5 and 0.45 at 110 and 115 GHz, respectively). Due to the nature of the OTF technique, spectra in pixels near the edges of the map have a significantly higher rms noise. Hence, an rms filter was applied to the combined map to blank pixels that had an rms noise of more than 3 times the mean rms noise for the entire map. Histograms showing the range of

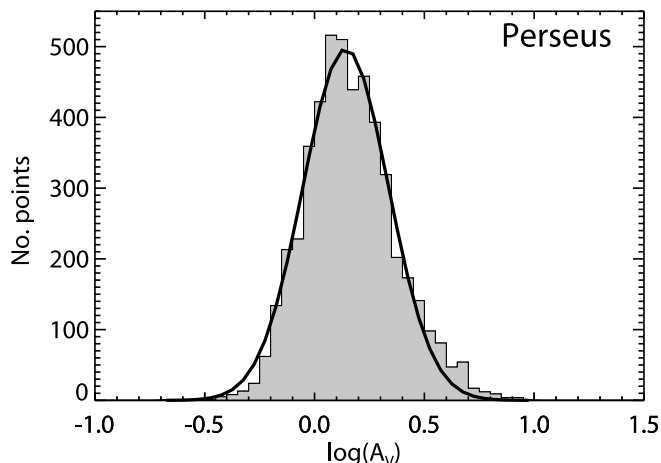
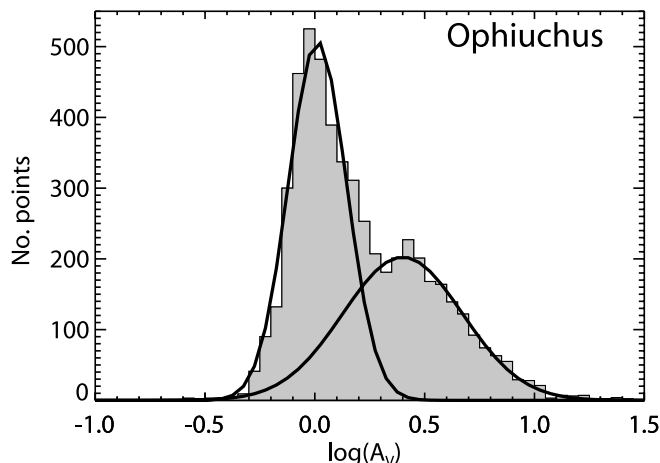


FIG. 8.—Histograms of extinction as derived from *IRAS* 60 and 100  $\mu$ m emission in Ophiuchus (*left*) and Perseus (*right*) for the areas shown in Figs. 3 and 4 (*histograms*) with a lognormal fit to the data overlotted (*curves*; in the case of Ophiuchus, a two-component fit was used).

<sup>21</sup> FCRAO is supported by NSF grant AST 02-28993.

<sup>22</sup> A rotation angle of 326° east of north was used as the scanning direction in the case of Perseus.



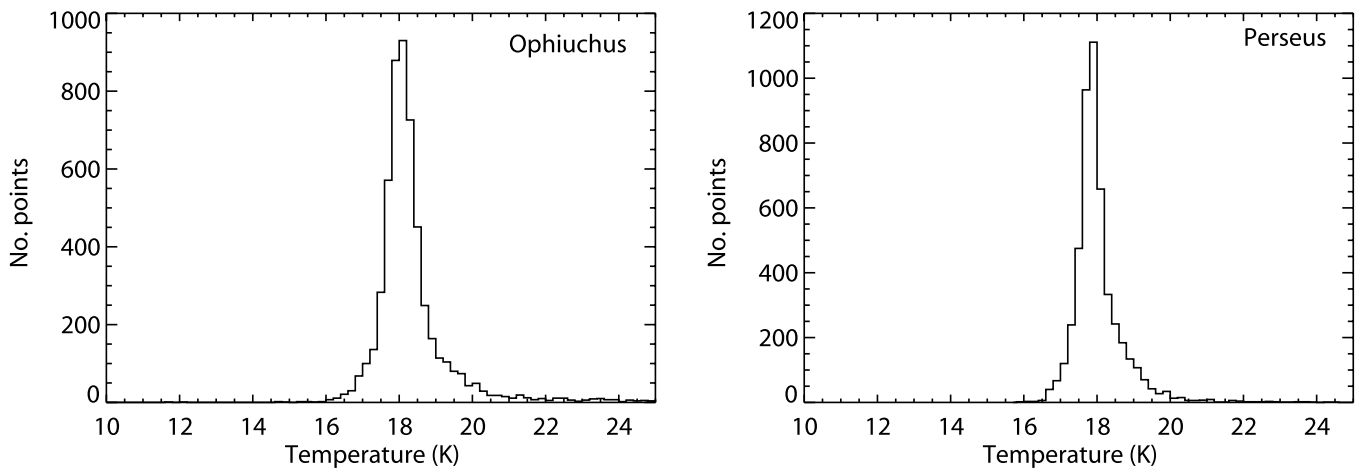


FIG. 9.—Histograms of temperature as derived from *IRAS* in Ophiuchus (*left*) and Perseus (*right*) for the areas shown in Figs. 3 and 4. Note that the relatively low resolution of these maps ( $\sim 5'$ ) means that we are not sensitive to the coldest, densest regions within the clouds, and hence the average temperature is somewhat higher than the  $\sim 10$  K more typically associated with molecular clouds.

rms noise in the final three-dimensional data cubes are presented in Figure 12.

The resolution, coverage, sampling, and sensitivity of the resulting data cubes are summarized in Table 6. Figure 13 shows average  $^{12}\text{CO}$  and  $^{13}\text{CO}$  spectra for Ophiuchus and Perseus, created by summing the spectra in all pixels for which the ratio of peak antenna temperature to rms noise is greater than 3.

Integrated intensity maps of  $^{12}\text{CO}$  and  $^{13}\text{CO}$  emission were made by summing over the range of velocities in which emission was seen. The integrated intensity maps of  $^{13}\text{CO}$  in Ophiuchus and Perseus are shown in Figures 14 and 15. The  $^{12}\text{CO}$  maps are not shown here but can be viewed online at the COMPLETE Web site.

Although extensive, the CO maps are more limited in areal coverage than the preceding data sets. For instance, the north-eastern filament and northwestern extension we see in the extinction map of Ophiuchus are not well sampled in CO emission. While the morphology generally follows that of the extinction map, a bright maxima north of the Oph A core within L1688 is quite prominent in the  $^{13}\text{CO}$  map of Ophiuchus. The average  $^{12}\text{CO}$  and  $^{13}\text{CO}$  spectra (Fig. 13, *left*) show an approximately Gaussian profile with a maximum width of  $\sim 7$  km s $^{-1}$ . Table 7 gives the central velocity and FWHM obtained by fitting a Gaussian profile to the average spectra.

The morphology of the integrated CO intensity in Perseus is again similar to that of the extinction, but due to their  $\sim 4$  times better linear spatial resolution over the extinction map, the  $^{12}\text{CO}$  and  $^{13}\text{CO}$  maps reveal complex substructure within the clumps we see in extinction. The CO emission shows components at multiple velocities and a steep velocity gradient across the cloud

complex, with a difference of almost 10 km s $^{-1}$  over the  $\sim 30$  pc east-west extent of the complex. This is the main cause of the wide line widths ( $\sim 15$  km s $^{-1}$ ) and non-Gaussian profiles exhibited by the average  $^{12}\text{CO}$  and  $^{13}\text{CO}$  spectra shown in Figure 13<sup>23</sup> and suggests that the Perseus complex is much more dynamic than Ophiuchus.

Histograms of the  $^{12}\text{CO}$  and  $^{13}\text{CO}$  integrated intensity are shown in Figure 16. Unlike the 2MASS NICER extinction maps, the distribution of CO intensities does not follow a lognormal distribution. In particular, there is a significant low-intensity tail to the distribution. In Perseus, the distribution also appears somewhat truncated on the high-intensity side. This is likely a result of a combination of chemical effects (e.g., freeze out) and the high optical depth of both  $^{12}\text{CO}$  and  $^{13}\text{CO}$  at higher column densities. The warmer temperatures (as traced by the *IRAS* temperature map) in the densest regions of Ophiuchus may prevent CO freezing out there.

<sup>23</sup> Multiple outflows in the region also contribute.

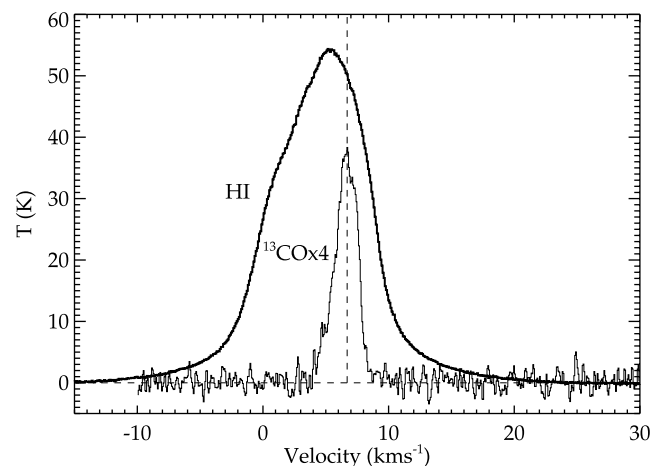


FIG. 10.—Spectra of H I and  $^{13}\text{CO}$  at the position of the dense core B1. The molecular gas (as traced by the  $^{13}\text{CO}$ ) has a peak velocity offset by  $\sim 2$  km s $^{-1}$  from the atomic gas. Both spectra are centered on the position 03<sup>h</sup>33<sup>m</sup>17<sup>s</sup>.8, +31<sup>o</sup>07'30" (J2000.0).

TABLE 5  
H I DATA

Parameter	Ophiuchus	Perseus
Pixel size (arcmin).....	4	4
HPBW (arcmin).....	9	9
Areal coverage (deg <sup>2</sup> ).....	5	20
1 $\sigma$ rms per channel (K).....	0.15	0.15
Spectral resolution (km s $^{-1}$ ).....	0.32	0.32

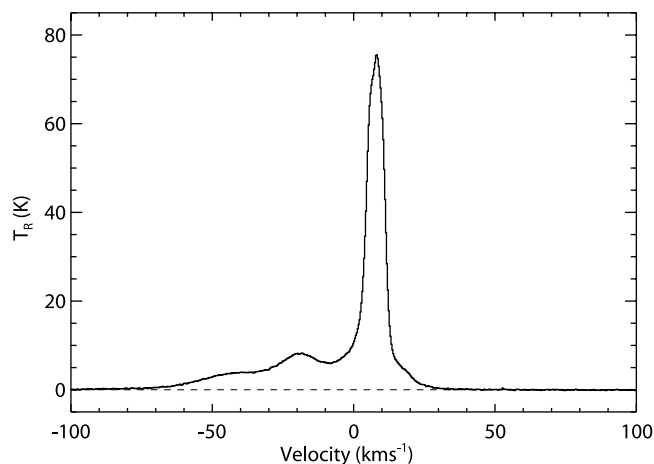


FIG. 11.—Spectrum of H I emission at the position  $03^{\text{h}}46^{\text{m}}21^{\text{s}}.6$ ,  $+33^{\circ}26'48''.5$  (J2000.0), showing an extended line wing and second component, possibly from another Galactic arm.

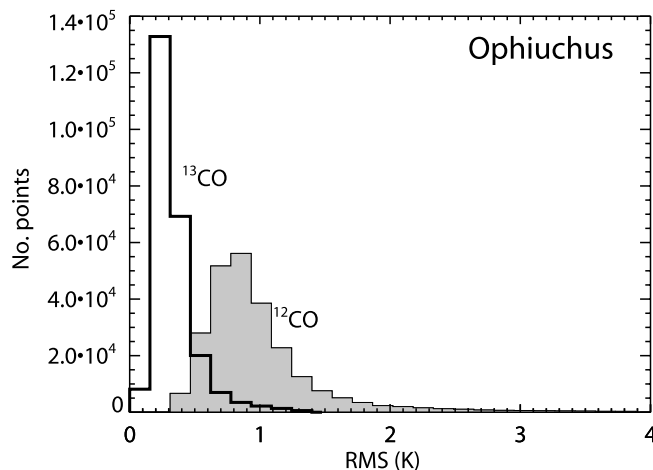
### 2.5. Thermal Dust Emission Maps from JCMT

Submillimeter continuum data at  $850\ \mu\text{m}$  of the Ophiuchus and Perseus molecular clouds were obtained using the Submillimeter Common User Bolometer Array (SCUBA) on the 15 m James Clerk Maxwell Telescope (JCMT)<sup>24</sup> on Mauna Kea, Hawaii. The data presented here are a combination of our own observations ( $\sim 5.6\ \text{deg}^2$  of Ophiuchus and  $\sim 1.3\ \text{deg}^2$  of Perseus) with publicly available archival data<sup>25</sup> for a total of  $\sim 5.8\ \text{deg}^2$  of Ophiuchus and  $\sim 3.5\ \text{deg}^2$  of Perseus.

All raw data were first flat-fielded and extinction-corrected using the standard SCUBA software (Holland et al. 1999). The data were then converted into images by applying the matrix inversion technique of Johnstone et al. (2000) with a pixel size of  $6''$ . Although the maps have an intrinsic beam size of  $14''$ , their effective beam size is  $19''.9$  because each was convolved with a  $\sigma = 6''$  Gaussian to reduce pixel noise. Structure on scales several times larger than the chop throw ( $>120''$ ) may be an artifact of image reconstruction (independent of the technique; see

<sup>24</sup> The JCMT is operated by the Joint Astronomy Centre in Hilo, Hawaii, on behalf of the parent organizations: the Particle Physics and Astronomy Research Council in the United Kingdom, the National Research Council of Canada, and the Netherlands Organization for Scientific Research.

<sup>25</sup> Guest User, Canadian Astronomy Data Centre, which is operated by the Dominion Astrophysical Observatory for the National Research Council of Canada's Herzberg Institute of Astrophysics.



Parameter	Ophiuchus	Perseus
Pixel size (arcsec).....	23	23
Total number of spectra.....	244874	214316
Areal coverage ( $\text{deg}^2$ ).....	10.0	8.7
$^{12}\text{CO}$		
HPBW (arcsec).....	46	46
Mean rms per channel <sup>a</sup> (K).....	0.98	0.35
Min. rms per channel (K).....	0.31	0.11
Spectral resolution ( $\text{km s}^{-1}$ ).....	0.064	0.064
$^{13}\text{CO}$		
HPBW (arcsec).....	44	44
Mean rms per channel <sup>a</sup> (K).....	0.33	0.17
Min. rms per channel (K).....	0.10	0.06
Spectral resolution ( $\text{km s}^{-1}$ ).....	0.066	0.066

<sup>a</sup> After blanking of pixels with an rms noise greater than 3 times the mean rms in the unblanked data file.

Johnstone et al. 2000). Large-scale artifacts were removed by subtracting a convolved version of the original map (made with a Gaussian of  $\sigma = 90''$ ) from each map. To minimize the occurrence of artificial negative “bowls” around bright sources resulting from this technique, all pixels with values  $>|5|$  times the mean noise were set to specifically  $+5$  or  $-5$  times the mean noise prior to convolution. Since each map was constructed from data obtained under a variety of weather conditions, the noise across each map is not uniform. The noise variation across each map, however, is typically only a factor of a few. The mean and rms standard deviation are  $\sim 40$  and  $20\ \text{mJy beam}^{-1}$ , respectively, in Ophiuchus and  $\sim 8$  and  $\sim 7\ \text{mJy beam}^{-1}$ , respectively, in Perseus. Due to their size, it is not possible to display the maps clearly in this work, and again we refer the reader to the COMPLETE Web site, where fits files are publicly available. The properties of the maps are summarized in Table 8.

Detailed analyses and images of the submillimeter maps are presented in Johnstone et al. (2004) for Ophiuchus and in Kirk et al. (2006) for Perseus or can be viewed online at the COMPLETE Web site, and so they are not repeated here. The positions of the dense clumps detected in the submillimeter are shown as red circles in Figures 14 and 15.

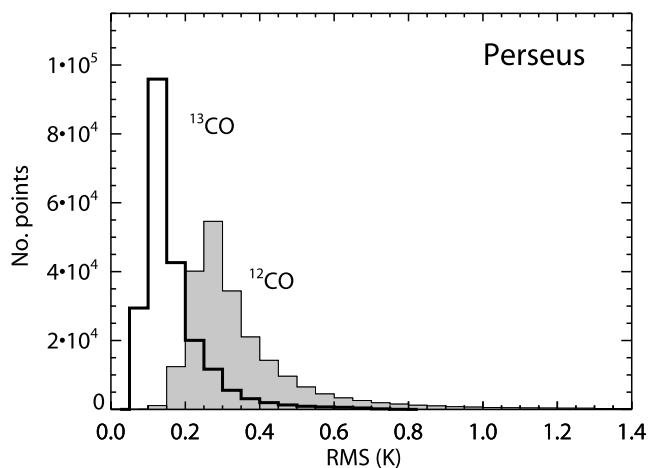


FIG. 12.—Histograms of rms noise per channel in the  $^{12}\text{CO}$  and  $^{13}\text{CO}$  maps of Ophiuchus (left) and Perseus (right).

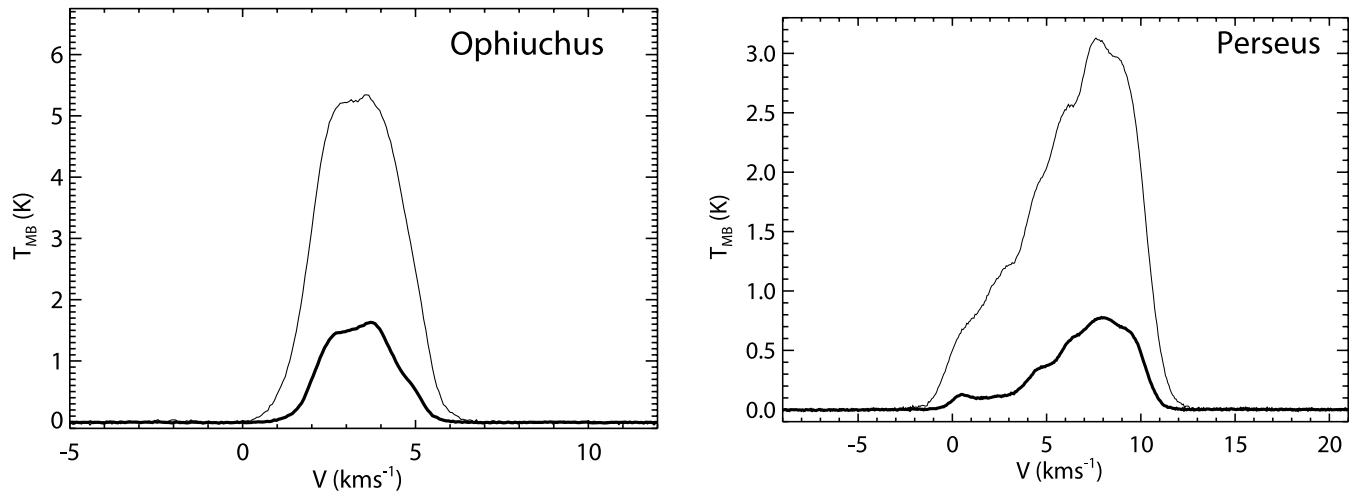


FIG. 13.— Average  $^{12}\text{CO}$  (*thin lines*) and  $^{13}\text{CO}$  (*thick lines*) spectra for Ophiuchus (*left*) and Perseus (*right*), created by summing the spectra in all pixels for which the ratio of peak antenna temperature to rms noise is greater than 3. The multicomponent nature of Perseus is clearly visible, while Ophiuchus displays a more Gaussian-like profile.

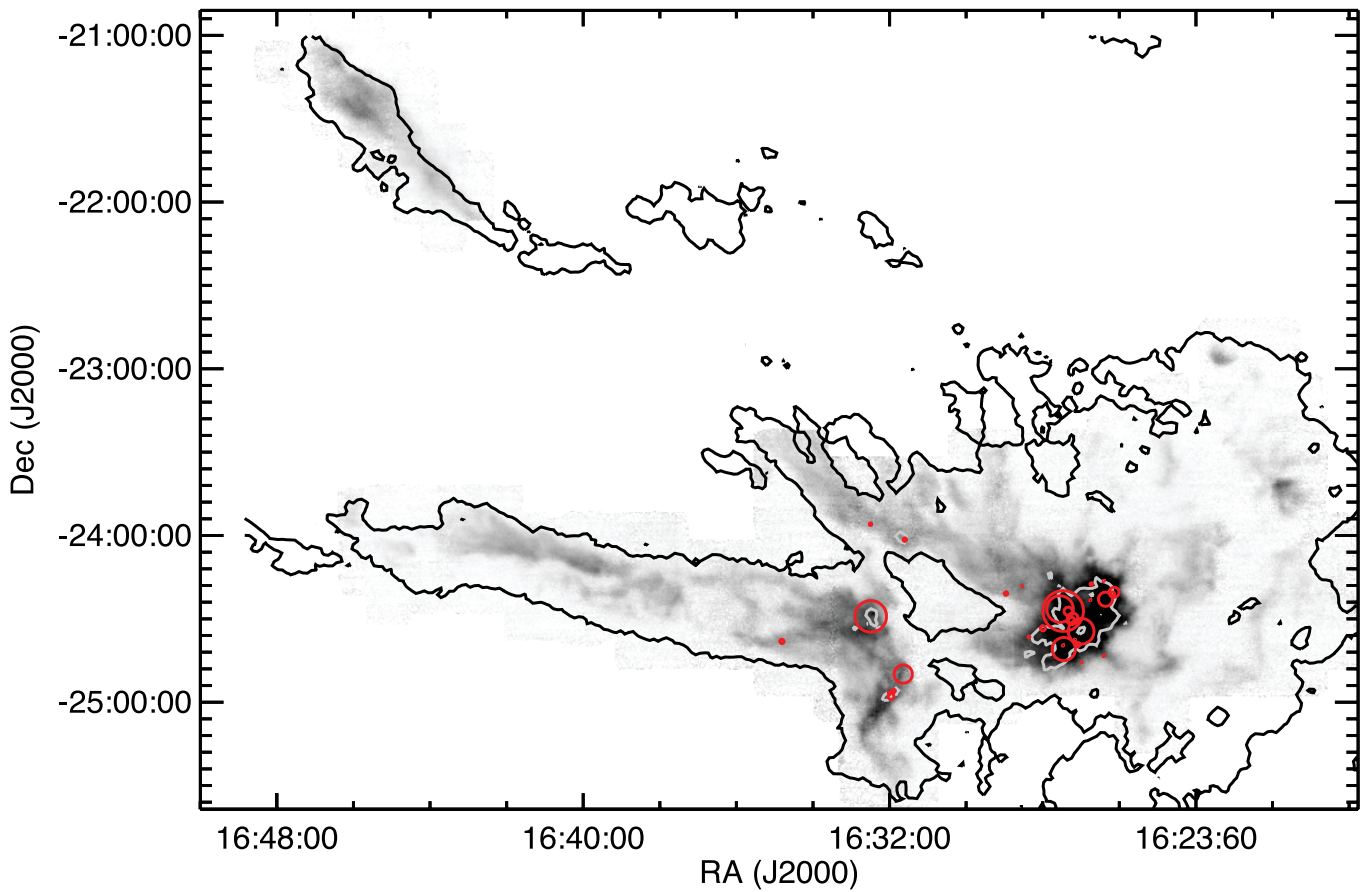


FIG. 14.— Integrated intensity image of  $^{13}\text{CO}$  emission in Ophiuchus, overlaid with the positions of the dense cores detected in submillimeter continuum emission (*red circles*; see § 2.5). Symbol size is proportional to the mass of the core. The black contour indicates  $A_V = 3$  mag from the 2MASS NICER map, and the gray contour indicates  $A_V = 15$  mag, the implied threshold for dense core formation in Ophiuchus.

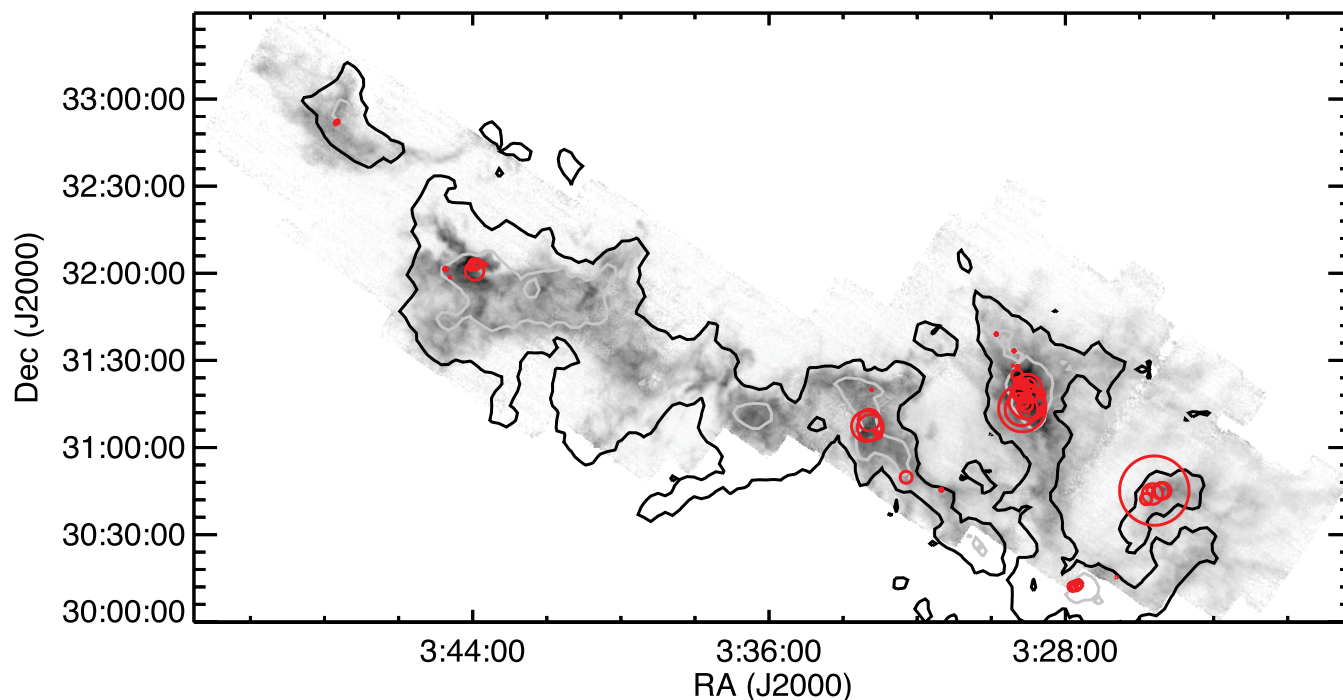


FIG. 15.— Integrated intensity image of  $^{13}\text{CO}$  emission in Perseus, overlaid with the positions of the dense cores detected in submillimeter continuum emission (*red circles*; see § 2.5). Symbol size is proportional to the mass of the core. The black contour indicates  $A_V = 3$  mag from the 2MASS NICER map, and the gray contour indicates  $A_V = 6$  mag, the implied threshold for dense core formation in Perseus.

Of particular interest in the Ophiuchus map is the lack of any submillimeter emission northwest of L1688, which was well covered with SCUBA as a result of the *IRAS*-based extinction map showing possible moderate extinction in that direction. This lack of detection is likely due to especially low sensitivity to extended, diffuse structures that may inhabit that location (see Johnstone et al. 2004). Also, as has been discussed in Johnstone et al. (2004), there appears to be a threshold of column density (extinction) below which no dense cores are found. In the case of Ophiuchus this threshold is at an  $A_V$  of  $\sim 15$  mag, as indicated by the gray contour in Figure 14.

As in Ophiuchus, all of the dense submillimeter clumps in Perseus are found to lie within the larger high-extinction regions, but the threshold of  $A_V \sim 5\text{--}7$  mag is somewhat lower than in Ophiuchus. This difference in thresholds cannot be attributed to the different sensitivities of the two submillimeter maps: this is

discussed further in Kirk et al. (2006). A similar threshold has also been reported by Hatchell et al. (2005) and Enoch et al. (2006).

### 3. SUMMARY

We have presented maps of the gas and dust in the Ophiuchus and Perseus star-forming regions, obtained using a range of different techniques and providing information on the star-forming material on scales of 0.1–10 pc. These observations complement the observations made as part of the *Spitzer Space Telescope* “From Molecular Cores to Planet Forming Disks” Legacy Program, which provides a catalog of the young stars.

Some highlights of the data are as follows:

1. The apparent morphology and distribution of star-forming material varies significantly between different column density tracers, with the near-infrared extinction method providing the

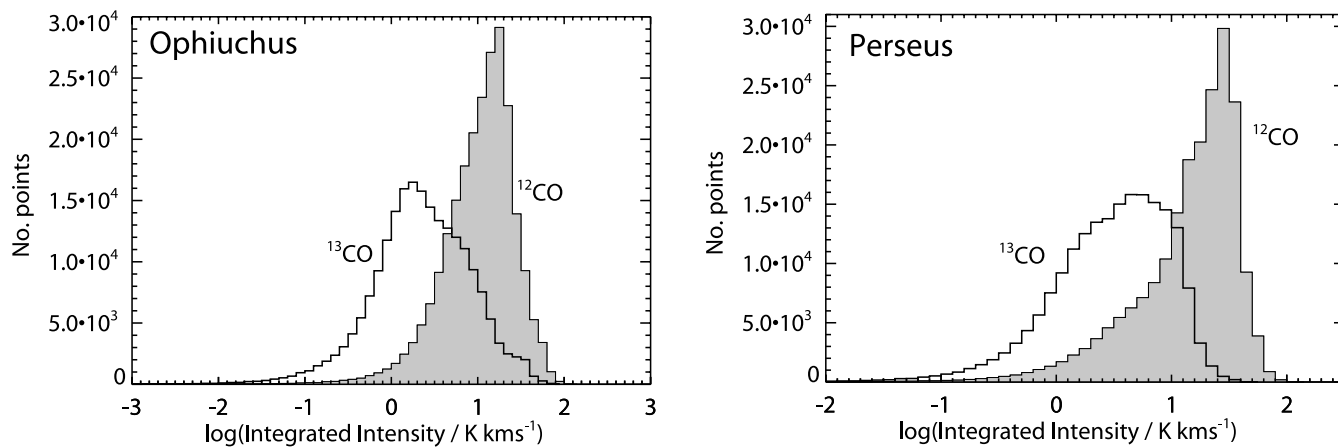


FIG. 16.— Histograms of  $^{12}\text{CO}$  and  $^{13}\text{CO}$  integrated intensity for Ophiuchus (*left*) and Perseus (*right*).

TABLE 7  
RESULTS OF GAUSSIAN FITS TO THE AVERAGE  $^{12}\text{CO}$   
AND  $^{13}\text{CO}$  LINES IN OPHIUCHUS

Line	FWHM ( $\text{km s}^{-1}$ )	$V_{\text{LSR}}$ ( $\text{km s}^{-1}$ )
$^{12}\text{CO}$ .....	2.77	3.38
$^{13}\text{CO}$ .....	2.38	3.38

closest match to the lognormal distribution of material predicted by numerical simulations.

2. CO emission in Ophiuchus shows approximately Gaussian line shapes, while Perseus appears much more dynamic, with multiply peaked, wide, non-Gaussian lines.

3. There appears to be an extinction threshold below which dense submillimeter cores are not detected. This threshold varies from region to region ( $A_V \sim 15$  mag in Ophiuchus and  $\sim 5\text{--}7$  mag in Perseus).

4. H I emission in Perseus shows an extremely high-velocity line wing, possibly reflecting emission from another Galactic arm.

All of the data sets presented here are publicly available from the COMPLETE Web site.

TABLE 8  
SCUBA 850  $\mu\text{m}$  CONTINUUM DATA

Parameter	Ophiuchus	Perseus
Pixel size (arcsec).....	6	6
Effective resolution (arcsec).....	19.9	19.9
Areal coverage ( $\text{deg}^2$ ).....	5.8	3.5
Mean rms noise <sup>a</sup> ( $\text{mJy beam}^{-1}$ ).....	40 (20)	8 (7)

<sup>a</sup> Values in parentheses are rms standard deviation.

N. A. R. is supported by the National Science Foundation through award AST 04-07172. J. B. F. is supported by the NASA ADP program. H. K. is supported by a National Research Council of Canada GSSSP award. D. J.'s research is supported by a grant from the Natural Sciences and Engineering Research Council of Canada. J. E. P. is supported by the National Science Foundation through grant AF002 from the Association of Universities for Research in Astronomy, Inc., under NSF cooperative agreement AST 96-13615 and by Fundación Andes under project C-13442. S. L. S. is supported by a National Science Foundation Graduate Research Fellowship.

#### REFERENCES

- Andersson, B. G., Wannier, P. G., Moriarty-Schieven, G. H., & Bakker, E. J. 2000, *AJ*, 119, 1325
- Arce, H. G., & Goodman, A. A. 1999a, *ApJ*, 512, L135
- . 1999b, *ApJ*, 517, 264
- de Geus, E. J., de Zeeuw, P. T., & Lub, J. 1989, *A&A*, 216, 44
- Enoch, M., et al. 2006, *ApJ*, 638, 293
- Evans, N. J., et al. 2003, *PASP*, 115, 965
- Goodman, A. A., & Heiles, C. 1994, *ApJ*, 424, 208
- Hatchell, J., Richer, J. S., Fuller, G. A., Quattrone, C. J., Ladd, E. F., & Chandler, C. J. 2005, *A&A*, 440, 151
- Heyer, M. H., Narayanan, G., & Brewer, M. K. 2001, On the Fly Mapping at the FCRAO 14 m Telescope (Amherst: Univ. Massachusetts), <http://www.astro.umass.edu/~fcrao/library/manuals/otfmanual.html>
- Holland, W. S., et al. 1999, *MNRAS*, 303, 659
- Indebetouw, R., et al. 2005, *ApJ*, 619, 931
- Johnstone, D., Di Francesco, J., & Kirk, H. 2004, *ApJ*, 611, L45
- Johnstone, D., Wilson, C. D., Moriarty-Schieven, G., Giannakopoulou-Creighton, J., & Gregersen, E. 2000, *ApJS*, 131, 505
- Kirk, H., Johnstone, D., & Di Francesco, J. 2006, *ApJ*, in press (astro-ph/0602089)
- Kutner, M. L., & Ulich, B. L. 1981, *ApJ*, 250, 341
- Lada, E. A. 1992, *ApJ*, 393, L25
- Li, D., & Goldsmith, P. F. 2003, *ApJ*, 585, 823
- Lombardi, M., & Alves, J. 2001, *A&A*, 377, 1023
- . 2006, *A&A*, in press
- Lombardi, M., Alves, J., & Lada, C. 2006, *A&A*, in press
- Lombardi, M., & Schneider, P. 2001, *A&A*, 373, 359
- Miville-Deschênes, M.-A., & Lagache, G. 2005, *ApJS*, 157, 302
- Ostriker, E. C., Stone, J. M., & Gammie, C. F. 2001, *ApJ*, 546, 980
- Ridge, N. A., Schnee, S. L., Goodman, A. A., & Foster, J. B. 2006, *ApJ*, in press (astro-ph/0601692)
- Rieke, G. H., & Lebofsky, M. J. 1985, *ApJ*, 288, 618
- Schnee, S. L., Bethell, T., & Goodman, A. A. 2006, *ApJ*, 640, L47
- Schnee, S. L., Ridge, N. A., Goodman, A. A., & Li, J. G. 2005, *ApJ*, 634, 442
- Walawender, J., Bally, J., Kirk, H., & Johnstone, D. 2005, *AJ*, 130, 1795
- Wood, D. O. S., Myers, P. C., & Daugherty, D. A. 1994, *ApJS*, 95, 457